Spectroscopic and Computational Studies of Aqueous Ethylene Glycol Solution Surfaces

Elizabeth L. Hommel, John K. Merle, Gang Ma, Christopher M. Hadad,* and Heather C. Allen*

Department of Chemistry, The Ohio State University, 100 West 18th Avenue, Columbus, Ohio 43210

The combination of Monte Carlo, ab initio, and DFT computational studies of ethylene glycol (EG) and EG−water hydrogen-bonding complexes indicate that experimental vibrational spectra of EG and EG−water solution surfaces have contributions from numerous conformations of both EG and EG−water. The computed spectra, derived from harmonic vibrational frequency calculations and a theoretical Boltzmann distribution, show similarity to the experimental surface vibrational spectra of EG taken by broad-bandwidth sum frequency generation (SFG) spectroscopy. This similarity suggests that, at the EG and aqueous EG surfaces, there are numerous coexisting conformations of stable EG and EG−water complexes. A blue shift of the CH_2 symmetric stretch peak in the SFG spectra was observed with an increase in the water concentration. This change indicates that EG behaves as a hydrogen-bond acceptor when solvated by additional water molecules. This also suggests that, in aqueous solutions of EG, EG−EG aggregates are unlikely to exist. The experimental blue shift is consistent with the results from the computational studies.

Introduction

Surfaces and buried interfaces have been recognized to play critical roles in the processing of molecules in the atmosphere, including pollutants.[1−5] Atmospheric aerosol surface chemistry, polar stratospheric cloud surface chemistry, and soil−water interfacial chemistry are examples of environmentally relevant processes at interfaces that are not well understood at the molecular level. The organization of molecules at various gas−liquid and solid−liquid interfaces is important to understand given that the orientation of the molecules can control the subsequent reaction pathways.

Many volatile organic compounds are detected at increasing levels in urban regions. These compounds are initially emitted as unsubstituted hydrocarbons, which are typically hydrophobic. As they react in the atmosphere with inorganic and other reactive species such as nitrates, sulfates, ozone, and other oxidizing agents, the hydrocarbons can gain functional groups resulting in a hydrophilic hydrocarbon. Ethylene glycol (1,2-ethanediol, EG) is a low-molecular-weight molecule with functionalities representative of hydrophilic secondary aerosols.[6] Thus, it was selected as an initial compound for the surface studies presented in this paper. Additionally, EG is used industrially to deice airplanes and airport runways, as well as in automobile antifreeze.[7−9] Consequently, a significant increase in the detection of EG is observed in the groundwater near airports during the winter months.[8,9]

In this study, broad-bandwidth sum frequency generation spectroscopy (BBSFG) is used to investigate neat liquid EG and aqueous EG liquid surfaces. Ethylene glycol has been shown to have numerous stable conformations[10] that can be observed by spectroscopic studies, and therefore, these experiments will directly probe the conformations that exist at the interface. In addition to the experimental techniques discussed here, a combination of Monte Carlo, ab initio, and density functional theory (DFT) calculations was employed to elucidate the conformations of the EG molecules and their complexes with water that can be located at the interface. The air−liquid interface comprises liquidlike and gaslike molecules, i.e., interfacial molecular aggregates. In recent years, clusters have been experimentally studied to better understand the liquid phase.[11] Yet, more importantly, clusters have been recognized to provide unique information about the air−liquid interface,[12,13] a medium that is different from the pure states of gas and liquid. The studies presented here allow us to directly compare clusters through computation with the air−liquid interface of EG and water through surface-selective optical spectroscopy to provide additional insight into the surface of an EG and water mixture. The nonlinear optical surface technique, utilized in these studies, BBSFG is sensitive to the molecular arrangement at the interface. Because the surface selectivity and the sensitivity to molecular arrangement, specifically surface orientation, is of significant interest, a brief introduction to the theory of vibrational SFG is given, followed by a brief discussion of the theoretical methods used.

Sum Frequency Generation. A brief overview of the theory of SFG is presented here, but a more in-depth discussion of SFG theory is available in the literature.[14] SFG is a second-order, nonlinear technique in which the macroscopic nonlinear susceptibility, $\chi^{(2)}$, is probed. SFG spectroscopy has been used to study a variety of surfaces and interfaces[12,13,15−20] because second-order nonlinear processes require the system to lack inversion symmetry. The interfacial region, by definition, meets this requirement. The SFG intensity, I_{SFG}, is given by eq 1a

$$I_{SFG} \propto |e_{SFG} \cdot \chi^{(2)} : e_{IR} e_{800}|^2 I(\omega_{IR}) \, I(\omega_{800}) \quad (1a)$$

$$\chi^{(2)} = \chi^{(2)}_{NR} + \sum_v \chi^{(2)}_v \quad (1b)$$

where I_{SFG} is proportional to the magnitude of the scalar product

* To whom correspondence should be addressed. E-mail: hadad.1@osu.edu (C.M.H.), allen@chemistry.ohio-state.edu (H.C.A.). Fax: 614-292-1685 (C.M.H.), 614-292-1685 (H.C.A.).

of the $\chi^{(2)}$ tensor with the exigent unit field vector, e_{SFG}, and the incident unit field vectors, $e_{IR}e_{800}$. The nonlinear macroscopic susceptibility, $\chi^{(2)}$, is described using both a nonresonant term, $\chi^{(2)}_{NR}$, and the sum of the resonant terms, $\chi^{(2)}_{v}$ (eq 1b). The resonant response dominates the nonlinear susceptibility when the frequency of an incident infrared beam, ω_{IR}, is resonant with the v vibrational level in the system. This resonance leads to the observation of a significant SFG enhancement. The resonant macroscopic nonlinear susceptibility, $\chi^{(2)}_{v}$, is given by eq 2

$$\chi_v^{(2)} \propto \frac{A_v}{\omega_v - \omega_{IR} - i\Gamma_v} \tag{2}$$

where A_v is the strength of the vth transition moment. The sign of A_v indicates whether the wavelength-overlapping SFG photons are 180° out of phase. The relative phase of the SFG photons gives rise to many features of the observed SFG spectrum. The phase is therefore critical to consider in the peak fitting because it strongly influences the shape of the spectral fit. The center frequency of the transition moment is represented by ω_v and the natural line width of the transition is Γ_v. The amplitude, A_v, includes both Raman and infrared contributions; therefore, SFG is observed only when the vibrational transition is both Raman and infrared active. To further illustrate this point, the molecular susceptibility, $\beta_{lmn,v}$, can be described by eq 3

$$\beta_{lmn,v} = \frac{\langle g|\alpha_{lm}|v\rangle\langle v|\mu_n|g\rangle}{\omega_{IR} - \omega_v + i\Gamma_v} \tag{3}$$

where $\langle g|\alpha_{lm}|v\rangle$ represents the Raman tensor for the transition and $\langle v|\mu_n|g\rangle$ represents the IR transition moment for the molecule. An Euler angle transformation relates the molecular coordinate system (l,m,n) to the laboratory coordinate system (I,J,K).[14,21−23] The transformation is given by eq 4

$$\beta_{IJK,v} = \sum_{lmn} \mu_{IJK:lmn} \beta_{lmn,v} \tag{4}$$

where $\mu_{IJK:lmn}$ is the Euler angle transformation between the laboratory coordinates (I,J,K) and the molecular coordinates (l,m,n). The macroscopic susceptibility, $\chi_{IJK,v}$, can be calculated from the molecular susceptibility, $\beta_{IJK,v}$, as shown in eq 5, where $\chi_{IJK,v}$ is equal to the number density, N, multiplied by the orientational average of $\beta_{IJK,v}$

$$\chi_{IJK,v}^{(2)} = N\langle\beta_{IJK,v}\rangle \tag{5}$$

Theoretical Methods

Structures. All quantum chemical calculations were performed using Gaussian 98[24] at the Ohio Supercomputer Center. Each of the 10 unique conformations of EG were optimized at the MP2/6-31+G** level and characterized as a minimum or saddle point at the same level via analytical vibrational frequency calculations. Complexes of EG with one water and of EG with two waters were obtained stochastically via a series of computational methods. Macromodel 7.0[25] was utilized to generate a diverse pool of 1000 EG−water complexes via a pseudo-Monte Carlo conformational search with the AMBER force field. The program Conformole[26] was used to evaluate all of the Monte Carlo structures for uniqueness, and this was determined by analyzing a series of molecular parameters, extracted by Conformole, including molecular energy and selected bond distances, bond angles, and torsion angles. Cases in which similar parameters were obtained were then inspected

visually. All unique complexes at the AMBER level were subsequently optimized at the HF/6-31G* level. The HF-optimized geometries were screened again for uniqueness using Conformole. The unique HF structures were optimized a final time at the MP2/6-31+G** level using the frozen-core approximation, and the resultant geometries were further screened for uniqueness. Each distinct complex was then confirmed to be a minimum on the potential energy surface (PES) via a vibrational frequency analysis at the MP2/6-31+G** level. Converged minima were characterized by having all real vibrational frequencies. Complexes corresponding to saddle points, i.e., those having imaginary vibrational frequencies, were displaced along the transition vector (typically 10%) in both directions and reoptimized via the opt=calcfc keyword. Reoptimized structures were then also analyzed for uniqueness. For purposes of comparison with experiment, Raman and IR intensities were calculated. The energy of each EG and EG−water complex was further evaluated via B3LYP/6-311+G** single-point energy calculations.[27−29] All basis sets used six Cartesian d functions. In a study of glycerol (1,2,3-propanetriol), Callam et al.[30] showed that B3LYP energies using a moderately sized basis set on HF or B3LYP geometries result in energetics that are in reasonable agreement with more expensive G2(MP2) and CBS-QB3 composite methods for the determination of conformational weightings for a Boltzmann distribution. MP2/6-31+G** zero-point vibrational energies were scaled by 0.9608.[31] All thermal corrections were determined using the harmonic oscillator, rigid rotor, and ideal gas approximations at 298 K.

Theoretical Spectra. For each of the systems (EG, EG plus one water, and EG plus two waters), a 298 K Boltzmann-weighted, theoretically derived, composite spectrum that utilized the calculated IR vibrational frequencies and product of Raman and IR intensities (proportional to the square of the transition moments) was then generated for comparison with the experimental surface sum frequency spectra of liquid EG and EG−water mixtures for the EG symmetric and asymmetric C−H stretching frequencies. It is important to note that an SFG spectrum is related to Raman and IR spectra through the respective matrix elements, i.e., the square of the product of the Raman and IR matrix elements. Phase differences between the symmetric and asymmetric stretching modes were assumed (for Figure 4, row 6), consistent with recent SFG work on the EG surface.[32] The weighting of each structure was determined via a Boltzmann average as shown in eq 6.[31]

$$N_i = \frac{g_i e^{(-G_i/k_B T)}}{\sum_i g_i e^{(-G_i/k_B T)}} \tag{6}$$

In eq 6, G_i is the free energy at 298 K of structure i at the B3LYP/6-311+G**//MP2/6-31+G** level relative to the structure with the lowest free energy set as zero, g_i is the structural degeneracy, k_B is Boltzmann's constant, and T is the temperature (298 K). Each C−H vibrational stretching frequency was simulated as a Lorentzian line shape with a full width at half-maximum (fwhm) of 20 cm^{-1}. The peak intensities were calculated to be the product of the IR intensity (km/mol) and Raman activity (Å^4/amu) as determined by the MP2/6-31+G** vibrational frequency calculations. Each MP2/6-31+G** C−H vibrational frequency was scaled by 0.937.[31]

Aqueous Ethylene Glycol Solution Surfaces

J. Phys. Chem. B, Vol. 109, No. 2, 2005 **813**

Experimental Methods

Instrumentation. The laser system used to obtain the BBSFG spectra has been previously described.[13,18−20,33] However, a brief overview is presented here with regard to the specific EG experiments that were performed. The BBSFG laser system includes two regenerative amplifiers [Spectra-Physics (SP), Spitfires]. The amplifiers are seeded with sub-50-fs, 800-nm pulses from a Ti:sapphire oscillator (SP, Tsunami). The amplifiers are pumped using a Nd:YLF laser (SP, Evolution30), operating at a 1-kHz repetition rate. One of the amplifiers produces 85-fs, 800-nm broadband pulses (∼300 cm^{-1}). The resulting broadband pulses then pump an optical parametric amplifier (SP, OPA-800C) to produce a broadband infrared beam (∼600 cm^{-1}, 1-kHz repetition rate). The second amplifier is equipped with a mask that spectrally narrows the pulse to 17 cm^{-1} (∼2 ps). The infrared beam energy was 13 μJ and the visible beam energy was 625 μJ. The infrared and the 800 nm beams were overlapped spatially and temporally on the liquid surface of interest. The resultant sum frequency signal was dispersed spectrally using a 500-mm monochromator equipped with a 1200 grooves/mm diffraction grating blazed at 750 nm (Acton Research, SpectroPro 500i), and the dispersed sum frequency light was collected using a liquid-nitrogen-cooled CCD camera (Roper Scientific, LN400EB, 1340 × 400 pixel array, back-illuminated CCD). The polarization conditions for the BBSFG spectra obtained were $S_{SFG}S_{vis}P_{IR}$ and $S_{SFG}P_{vis}S_{IR}$ ($P_{SFG}P_{vis}P_{IR}$ was also obtained, but not shown here). S-polarized light contains the electric field perpendicular to the plane of incidence, and P-polarized light is in the plane of incidence. The polarization of the 800-nm beam was selected using a zero-order waveplate. A Glan laser polarizer was used to verify the resultant BBSFG polarization. The $S_{SFG}S_{vis}P_{IR}$ spectra were obtained during 30-s acquisitions, and two spectra were averaged. The $S_{SFG}P_{vis}S_{IR}$ spectra were obtained during 5-min acquisitions to improve the signal-to-noise ratio, and two spectra were averaged. The SPS BBSFG spectra presented were normalized to be comparable to the 30-s-acquisition-time spectra. Before the BBSFG spectra were collected from the samples, a nonresonant BBSFG spectrum from the surface of a GaAs crystal was obtained during each experimental session. The BBSFG spectra, which are then normalized with the GaAs spectrum, show a central region where the peaks are easily discernible above the noise (∼400 cm^{-1}). As one would expect, the edges of these normalized spectra are dominated by noise; thus, only the central region was used for data presentation and interpretation.

The BBSFG spectra were calibrated using a polystyrene thin film and another nonresonant BBSFG spectrum from the same GaAs crystal. The calibration BBSFG spectrum was collected by placing a thin film of polystyrene (infrared absorbances are well-known) in the path of the infrared beam prior to beam overlap on the GaAs crystal. The resultant infrared beam is structured because of absorbance by the polystyrene film, which leads to a structured nonresonant BBSFG spectrum from the GaAs crystal. The peak positions (dips) in the calibration GaAs BBSFG spectrum are used to calibrate the BBSFG spectra obtained during the same experimental session.

The surface tension (ST) was measured using both the Wilhelmy method (Kibron Inc.) and the capillary rise method for the EG and aqueous EG solutions at 23°C. The solutions were contained in Teflon wells for the Wilhelmy ST measurements. Surface tension measurements were then used to calculate the surface number density (i.e., the surface mole fraction, X_{SEG}) for EG.

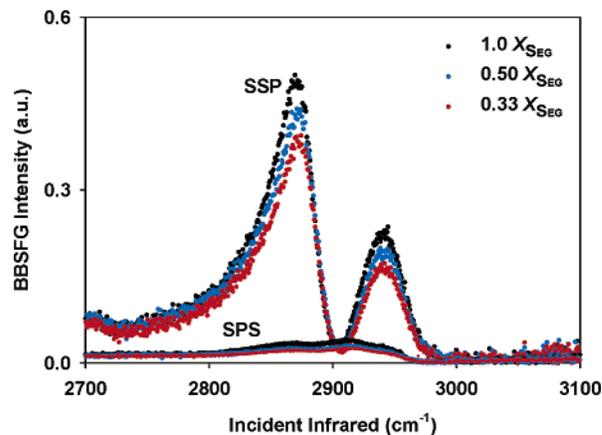A Thermo Nicolet FT-IR spectrometer (Avatar 370, Thermo Electron Corporation) was used for attenuated total reflection

Figure 1. Surface sum frequency spectra of ethylene glycol−water solutions using $S_{SFG}S_{vis}P_{IR}$ and $S_{SFG}P_{vis}S_{IR}$ polarization conditions. Concentrations are shown for the surface mole fraction of ethylene glycol, X_{SEG}.

FTIR (ATR-FTIR) spectroscopy. The ATR measurements were made on a silicon crystal using a 45° single-bounce ATR accessory (Foundation Series, Thermo Electron Corporation). Spectra were collected with a spectral resolution of 4 cm^{-1}, and 128 scans were averaged.

Raman spectra were obtained using 48 mW from a 532-nm continuous-wave laser (SP, Millennia II), a 500-mm monochromator (Acton Research, SpectroPro 500i, 600 grooves/mm grating blazed at 1 μm), and a liquid-nitrogen-cooled CCD camera (Roper Scientific, LN400EB, 1340 × 400 pixel array, back-illuminated, deep depletion CCD). Raman spectra were collected using a fiber optic (Inphotonics, RP 532-05-15-FC) that was coupled to the entrance slit of the monochromator. The slit width was set to 10 μm, and the resulting spectral resolution was 0.8 cm^{-1}. The Raman spectra were acquired with 30-s exposures to the CCD.

Chemicals. EG was purchased from Aldrich with a purity of 99.8% and used as received. Nanopure water with a resistivity of 18 MΩ cm was also used. The bulk mole fraction (X_{EG}) solutions were prepared by mass addition of both components into amber jars. The BBSFG spectra were collected using glass Petri dishes cleaned with ammonium persulfate sulfuric acid solution, rinsed with copious amounts of Nanopure water, and then dried in an oven.

Results and Discussion

A series of aqueous EG solutions with different EG concentrations was investigated, and six representative surface BBSFG spectra (SSP- and SPS-polarized) are shown in Figure 1 for neat EG and 0.50 and 0.33 X_{SEG} (surface mole fraction).[34] The 0.33 X_{SEG} solution has the lowest BBSFG response, and the neat EG has the strongest BBSFG response. The relative intensity of the BBSFG response increases with the concentration of EG for the SSP spectrum peaks in Figure 1. The peak observed in the SSP and SPS spectra around 2870 cm^{-1} is attributed to CH$_2$ symmetric stretching (CH$_2$-SS) modes, and the peak observed around 2950 cm^{-1} is attributed primarily to CH$_2$ asymmetric stretching (CH$_2$-AS) and, to a lesser extent, the Fermi resonance modes on the high-energy side of this peak. In the SPS spectra, the intensity observed around 2900 cm^{-1} is attributed to asymmetric stretching modes. The assignments are consistent with previously published Raman, IR, and SFG studies on EG,[32,35,36] and the calculations presented in this paper.

Because SFG data convolute surface number density with surface orientation, the surface tension of a series of aqueous
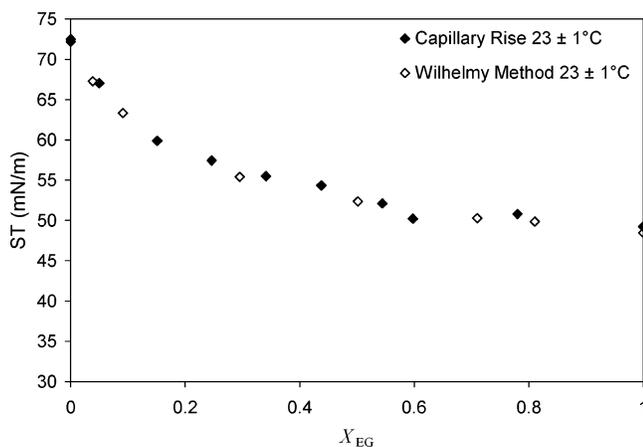
814 *J. Phys. Chem. B, Vol. 109, No. 2, 2005*

Hommel et al.

Figure 2. Surface tensions of ethylene glycol−water solutions. The surface tension was measured using both capillary rise (◆) and Wilhelmy (◇) methods at 23 °C.
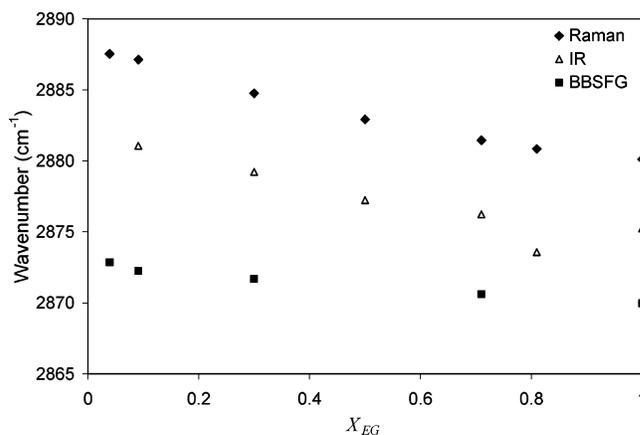

Figure 3. Raman, IR, and sum frequency generation vibrational frequencies for the CH_2 symmetric stretching modes of ethylene glycol versus the mole fraction of ethylene glycol in water.

EG solutions was measured to reveal the surface number density. Surface tension data from the EG−water solutions are plotted in Figure 2 versus the bulk mole fraction of the corresponding solution. The surface tensions of all of the EG solutions are lower than that of water ($ST_{H_2O} = 72.5$ mN/m at 23 °C). In the low-concentration regime for EG, the relative decrease in surface tension is greater than the relative change in the middle of the concentration range. Around 0.5 X_{EG} (bulk mole fraction) and higher, the surface tension is nearly constant with changes in the bulk concentration, and the curve approaches an asymptotic limit. This behavior suggests that, around 0.5 X_{EG}, the EG molecules nearly cover the surface and the surface number density of EG remains nearly unchanged for $X_{EG} > 0.5$. However, our BBSFG results (all data not shown here) indicate that the SFG intensity of the surface of the EG solutions increases throughout the full EG concentration regime. Because the SFG intensity is proportional to the square of the surface number density and to the surface orientation, the SFG intensity change is attributed to a surface orientation change when the surface density remains constant. Therefore, in the high-EG-concentration regime ($X_{EG} > 0.5$), the surface is experiencing an evolving rearrangement.

To fully understand how the surface structures of EG are similar to or different from the liquid-phase structures, additional Raman and IR studies were completed and then analyzed and compared to the surface SSP and SPS BBSFG spectral analysis. The CH_2-SS peak position was determined for Raman, IR, and BBSFG measurements of EG versus the bulk mole fraction of the corresponding EG solution, as shown in Figure 3. The Raman CH_2-SS peak is found at the highest wavenumber. The IR and BBSFG CH_2-SS peaks occur at lower wavenumbers. Furthermore, the Raman and IR measurements show an increase in the wavenumber (blue shift) with increasing water concentration of the solution. This trend was also observed in the BBSFG spectra, but to a lesser extent.

The blue shift that occurs because of solvation of EG by water is attributed to an increase in hydrogen bonding between water and EG. Previous spectroscopic studies of methanol−water solutions revealed a blue shift of the C−H stretches when methanol acts as a hydrogen-bond acceptor.[13] Although ethylene glycol has a propensity toward internal hydrogen bonding,[10] water can hydrogen bond efficiently with EG, thus disrupting the OH−OH EG intramolecular hydrogen bonding.

EG is a relatively simple molecule; however, its condensed-phase structures are quite complicated. Previous studies have shown that EG has numerous stable conformations[10] that can contribute to the observed vibrational spectra. Moreover, in addition to hydrogen bonding with itself, EG can form hydrogen-bonded complexes with water. Therefore, the BBSFG spectra of EG might have contributions from different conformations and different hydrogen-bonding structures as a function of mole fraction in solution.

To further investigate the effect of hydrogen bonding due to water and to understand which conformations contribute to the observed BBSFG spectra, computational methods were employed. Cartesian coordinates, vibrational frequencies, and molecular energies for the EG, EG with one water and EG with two water complexes are provided in Tables S.1 and S.2 (Supporting Information). The structural degeneracy, electronic plus zero-point vibrational energies (H_0), 298 K free energies (G_{298}), and relative percentages based on 298 K Boltzmann weightings are listed in Table S.3 (Supporting Information) for all of the gas-phase ethylene glycol conformations at the MP2/6-31+G** and B3LYP/6-311+G**//MP2/6-31+G** levels. One thousand unique EG and water complexes were generated and evaluated. Twenty of these complexes were found to contribute to the overall spectra. With regard to nomenclature, each EG conformation can be categorized on the basis of the dihedral angles for the H−O−C−C, O−C−C−O, and the C−C−O−H units of EG. The designations are g+ (gauche clockwise), g− (gauche counterclockwise), and t (trans), respectively, for the three dihedral angles. The O−C−C−O dihedral angle is capitalized by convention.

In the gas phase, the MP2/6-31+G** g−G+g− conformation corresponds to a first-order saddle point. Walking down either side of the maximum leads to a tG+g− minimum. Therefore, at the level of theory used in this work, the g−G+g− conformation does not contribute to the composite theoretical gas-phase spectrum. To our knowledge, this is the first post-HF ab initio computational study of isolated EG employing a basis set with diffuse functions on heavy atoms to optimize the geometries, and this approach appears to be the origin of the difference in this study as compared to those in the literature. Bultinck et al.[37] found the g−G+g− rotamer to be a minimum at the HF/6-31++G** level. Csonka and Csizmadia,[38] using HF and several DFT methods without diffuse functions in their basis sets, showed that the g−G+g− rotamer exists in a very shallow well. Other computational studies for the geometry optimizations of EG have been carried out with basis sets lacking diffuse functions.[10,39−41] A limited microsolvation study of EG complexed to water was recently reported while this work was in process.[42] However, our results, generated by a stochastic and

Aqueous Ethylene Glycol Solution Surfaces

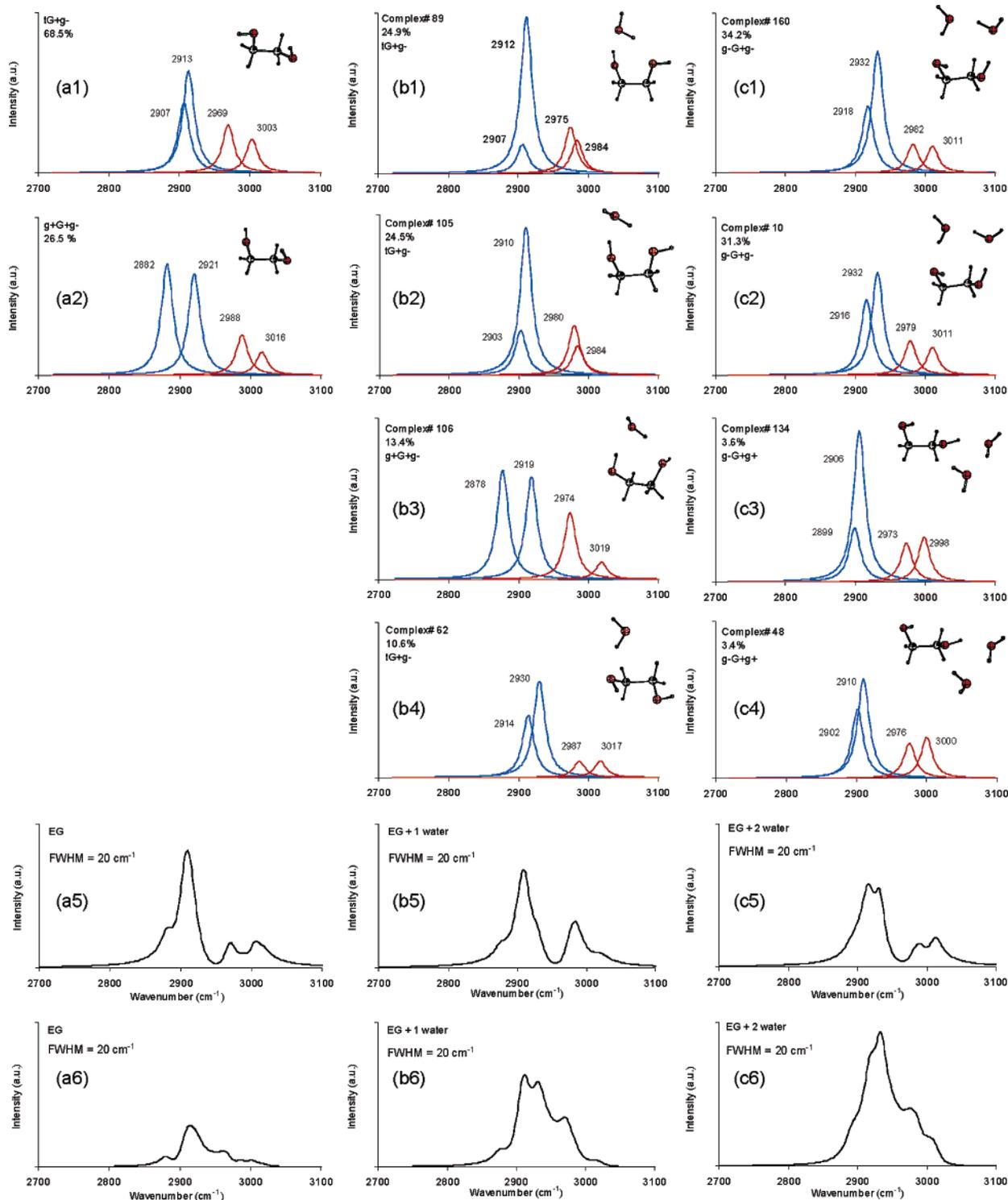*J. Phys. Chem. B, Vol. 109, No. 2, 2005* **815**

Figure 4. Calculated component peaks where the IR intensity is multiplied by the Raman intensity are shown in the first four rows. Column 1 contains the calculated peaks for neat ethylene glycol. Column 2 contains an ethylene glycol molecule complexed with one water molecule. Column 3 contains an ethylene glycol molecule complexed with two water molecules. Rows 5 and 6 show the calculated composite spectra that comprise the individual conformations weighted by the Boltzmann distribution, where at least a 90% distribution is included and a bandwidth of 20 cm^{-1} was used. Row 5 spectra show the symmetric and asymmetric stretches as in phase, and row 6 spectra show the symmetric and asymmetric stretches as out of phase.

random generation of starting structures, represents a more complete and thorough description of microsolvation in this system.

Figure 4 shows several spectra calculated using the SFG equations discussed above with the calculated Raman and IR oscillator strengths for the C–H stretching vibrational frequencies for various EG conformations, both in isolation and when complexed with water. Column a in Figure 4 corresponds to isolated EG, column b corresponds to complexes of EG with one water molecule, and column c corresponds to complexes of EG with two water molecules. Figure 4a1 shows a calculated spectrum of EG in the tG$^+$g$^-$ (trans torsional angle of H–O–C–C, gauche clockwise torsional angle of O–C–C–O, gauche counterclockwise torsional angle of C–C–O–H) conformation.

The tG$^+$g$^-$ conformation represents 68.5% of the calculated 298 K conformational distribution of EG molecules. Figure 4a2 shows the calculated spectrum of EG in the g$^+$G$^+$g$^-$ conformation. The g$^+$G$^+$g$^-$ conformation represents 26.5% of the calculated 298 K conformational distribution of EG molecules. Figure 4a5 shows a composite (Raman-IR) theoretical spectrum of EG using a fwhm of 20 cm^{-1} when the components of the tG$^+$g$^-$ and g$^+$G$^+$g$^-$ conformations (accounting for 95% at 298 K) are weighted and then combined according to eq 3, with the component peaks from the symmetric and asymmetric stretch modes having the same phase. The composite spectrum of EG with the component peaks from the symmetric and asymmetric stretch modes having opposite phase was generated and is shown in Figure 4a6. The out-of-phase character of the two types of stretching modes, symmetric and asymmetric, was incorporated by assigning a positive sign to the symmetric stretch component peak terms and a negative sign to the asymmetric stretch component peak terms. As shown in eqs 1−5, the sign change creates cross terms that take into account the interference that is observed in SFG spectra and is therefore necessary to consider for the calculated spectra as well.

Spectrum b1 in Figure 4 corresponds to the tG$^+$g$^-$ conformation of EG complexed with one water molecule (complex 89, Table S.2.). The tG$^+$g$^-$ conformation represents 24.9% of the calculated conformational distribution at 298 K of EG−one water complexes. Spectrum b2 also corresponds to the tG$^+$g$^-$ conformation of EG complexed with one water molecule (complex 105); however, the orientation of the water molecule has been changed, via rotation, to distinguish complex 105 from complex 89. Complex 105 represents 24.5% of the calculated conformational distribution at 298 K of EG−one water complexes. Spectrum b3 is for the g$^+$G$^+$g$^-$ conformation of EG with one water molecule (complex 106) and represents 13.4% of the calculated conformational distribution at 298 K of EG−one water complexes. Spectrum b4 is for another variation of the tG$^+$g$^-$ conformation of EG complexed with a water molecule (complex 62) and represents 10.6% of the calculated conformational distribution at 298 K of EG−one water complexes. These four spectra comprise the majority of the 298 K Boltzmann distributions. The stochastic procedure described in the Theoretical Methods section resulted in 21 unique complexes for EG with one water molecule. The total degeneracy of each complex was calculated to be the product of the degeneracy for the lone EG conformation and the degeneracy of the complex based on the number of possible identical complexes. The composite theoretical spectrum for the EG plus one water molecule consists of eight complexes that account for 91% of the Boltzmann distribution and is shown in spectrum b5 with a fwhm of 20 cm^{-1} with the component peaks from the symmetric and asymmetric stretch modes in phase. Spectrum b6 shows the same as b5, but with the symmetric and asymmetric stretching component peaks out of phase.

In Figure 4, spectrum c1 corresponds to the g$^-$G$^+$g$^-$ conformation of EG complexed with two water molecules (complex 160, Table S.2.). Complex 160 represents 34.2% of the calculated conformational distribution at 298 K of EG−two water complexes. Spectrum c2 is also for the g$^-$G$^+$g$^-$ conformation of EG complexed with two waters (complex 10). Complex 10 is a variation of complex 160 in which one of the complexed waters has been rotated relative to the one in complex 160. Complex 10 represents 31.3% of the calculated conformational distribution at 298 K of EG−two water complexes. Spectrum c3 is for the g$^-$G$^+$g$^+$ conformation of EG complexed with two waters (complex 134, Table S.2) and

represents 3.6% of the calculated conformational distribution at 298 K of EG−two water complexes. Spectrum c4 is that for complex 48. Complex 48 differs from complex 134 via a rotated water molecule. Complex 48 represents 3.4% of the calculated conformational distribution at 298 K of EG−two water complexes.

The stochastic procedure described in the Theoretical Methods section resulted in 57 unique complexes for EG with two water molecules. The total degeneracy of each complex was calculated to be the product of the degeneracy for the lone EG conformation and the degeneracy of the position of the waters based on the EG conformation symmetry and water exchange. The composite theoretical spectrum for the EG complexes with two water molecules consists of 12 complexes, accounting for 91% of the Boltzmann distribution as shown in spectrum c5 of Figure 4 using a fwhm of 20 cm^{-1} with the component peaks from the symmetric and asymmetric stretch modes in phase. Spectrum c6 of Figure 4 is similar to spectrum c5, but the component peaks from the symmetric and asymmetric stretch modes were generated by incorporating their relative phases (eqs 1 and 2).

The large peak (between 2900 and 2930 cm^{-1}) observed in the theoretical composite spectra shown in row 5 of Figure 4 encompasses the CH$_2$-SS modes for the conformers contributing to the spectra. The peaks above 2950 cm^{-1} are attributed to the CH$_2$-AS modes. The one water molecule complex with the EG molecule causes a minimal blue shift, whereas the two water molecule complex with the EG molecule causes a larger blue shift ($\sim$15 cm^{-1}).

The theoretical composite spectra shown in row 5 of Figure 4 resemble the SSP BBSFG spectra collected and shown in Figure 1. However, it is more accurate to compare the composite spectra that incorporates the phase differences shown in row 6 of Figure 4 to both the SSP and SPS BBSFG spectra given that additional intensity from asymmetric stretching modes appears in the SPS BBSFG spectra of neat EG and EG solutions. To further illustrate this point, the computational out-of-phase (Figure 4, row 6) and experimental SSP- and SPS-polarized spectra are shown in Figure 5 for direct comparison as a function of surface mole fraction based on the surface tension data: (a) neat EG, (b) one EG−one water, and (c) one EG−two waters. The similarities between the calculated and the SSP and SPS BBSFG experimental spectra suggests that the EG−water surfaces are composed of several EG conformations and EG−water complexes, all of which contribute to the overall observed spectra. The calculated and experimental spectral similiarities within Figure 5b and c are primarily derived from the hydrogen bonding effects within the EG + one water and EG + two water complexes. In Figure 5a, the calculated spectrum is that of the EG monomer, and hydrogen bonding is not considered. Yet, it is a factor for the neat EG solution and is therefore a factor in the experimental spectra of Figure 5a. The hydrogen bonding between EG molecules is largely responsible for the differences observed between the calculated and experimental spectra of Figure 5a. In addition, differences in the experimental and the computed spectra of Figure 5a−c might be due to Fermi resonances.

The relative orientation of the molecules to an actual surface was not considered in the calculations; this is the reason for comparison of the calculated spectra to both the SSP and the SPS experimental spectra. (PPP-polarized BBSFG spectra were also obtained and are similar to the SPS spectra, but with higher intensities.) Mode interferences between the symmetric and asymmetric stretches were considered by incorporating relative phase effects using eqs 1 and 2. The interference effects provide
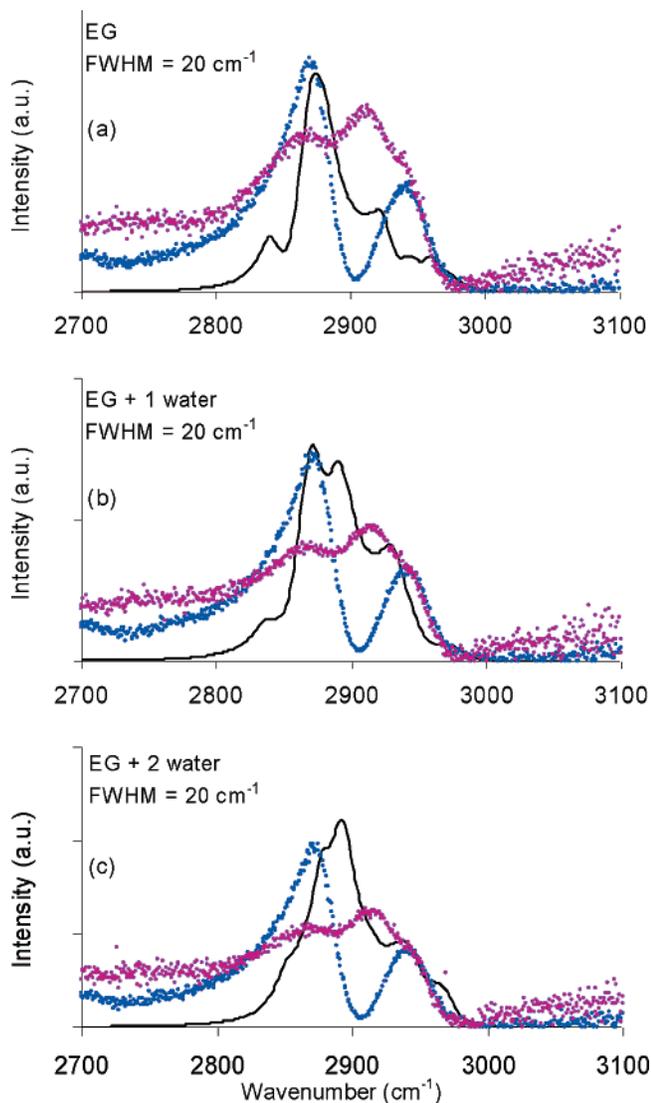
Aqueous Ethylene Glycol Solution Surfaces

J. Phys. Chem. B, Vol. 109, No. 2, 2005 **817**

Figure 5. Overlay of the experimental $S_{SFG}S_{vis}P_{IR}$- and $S_{SFG}P_{vis}S_{IR}$-polarized BBSFG and calculated out-of-phase (+ symmetric, − asymmetric modes; Eqns. 1−5) composite spectra for (a) neat EG, (b) $X_{SEG} = 0.5$ (one EG−one H$_2$O), (c) $X_{SEG} = 0.33$ (one EG−two H$_2$O). For each spectrum, the peak intensity for the symmetric stretch below 2900 cm^{-1} was normalized to the calculated intensity for that peak. For overlay (a), a scaling factor of 0.987 was used for the calculated EG spectral x-axis in order to coincide the calculated and the experimental maximum for the symmetric stretching peak. In each of the other spectra, the same scaling factor of 0.987 was utilized for the calculated spectral x axes.

additional intensity in the calculated spectra (Figure 4, row 6, and Figure 5) that also compares favorably with the asymmetric stretch intensity observed in the SPS-polarized spectra shown in Figures 1 and 5. (Figure 5a−c SPS spectral intensities were increased by a factor of 10.) The observed intensity in the 2900 cm^{-1} region of the out-of-phase calculated spectra (Figure 5a−c) supports the suggestion that EG molecules at the liquid surface are present in many different conformations. These conformers, as illustrated in Figure 4, are accountable for the changes in the calculated spectra (Figure 4, rows 5 and 6), and describe, reasonably well, the contributions to the experimental SSP and SPS surface spectra. In particular, there is reasonable agreement between the calculated intensity for both the symmetric and asymmetric C−H stretches in the EG plus one water molecule spectra (Figure 5b). Indeed, the out-of-phase calculated spectra for a surface mole fraction of 0.5 appear to represent

the relative intensities within the SSP and SPS experimental spectra also shown in Figure 5b. This agreement suggests that a single water molecule and an EG molecule can act as suitable surrogates for each other when complexed to an EG molecule at the surface. Finally, Figure 5c shows the experimental spectrum for a surface mole fraction of 0.33 (EG with two water molecules) and compares that spectrum to the calculated intensities for the Boltzmann-averaged complexes of EG with two waters. The agreement between experiment and theory in Figure 5c is less good with respect to the overlap of the symmetric stretch peak.

These results and comparisons suggest that, at the surface, EG is effectively complexed with water. Furthermore, the effect of hydrogen bonding between the EG and water molecules on the spectra can be seen when spectrum a1 of Figure 4 is compared with spectra b1, b2, and b4, where they are all the same tG$^+$g$^-$ conformation and vary by the presence and orientation of water. The calculated predominance of the tG$^+$g$^-$ conformation also suggests that it is not appropriate to calculate relative orientation angles of the EG methylene moieties at the surface as such calculations assume a delta distribution of orientation for both methylene groups. In addition to the comparisons of spectral intensity, a blue shift of the symmetric stretch frequencies is observed in both the calculated (component peaks in Figure 4, rows 1−4), and the experimental surface and bulk (Figure 3) spectra. This is consistent with increased hydrogen bonding between EG and water within the EG−water complexes as opposed to intramolecular EG−EG hydrogen bonding as water is added to the solution.

Conclusions

The computational analysis of EG and EG complexes with water in addition to the surface spectra strongly suggests that EG−water surfaces comprise multiple conformations of EG and EG−water complexes. Moreover, ≤4 conformational complexes are shown to describe the observed surface vibrational spectra reasonably well. The surface spectra in addition to surface tension measurements reveal that the methylene groups of EG undergo a rearrangement at their solution surface for bulk mole fractions greater than 0.5 EG. At high water concentrations (low EG contents), EG acts as an efficient hydrogen-bond acceptor as compared to higher EG concentrations. This is indicated by both the computational and the vibrational spectroscopic results for the surface and the liquid-phase studies. At the surface, as water is added to a neat EG liquid, EG is complexed to the solvating water molecules. This also suggests that water successfully competes against other EG molecules for complexation with an EG molecule, which is observed from the shift to higher wavenumbers of the symmetric stretch peaks of the calculated and the experimental spectra. This further indicates that EG−EG aggregates are unlikely to exist at aqueous EG solution surfaces.

Supporting Information Available: Absolute energies and enthalpic and free energy corrections to 298 K values, as well as moments of inertia for all structures and complexes, are provided. In addition, optimized Cartesian coordinates and

818 *J. Phys. Chem. B, Vol. 109, No. 2, 2005*

Hommel et al.

calculated harmonic vibrational frequencies are listed for all structures and complexes. This information is available free of charge via the Internet at http://pubs.acs.org.

References and Notes

(1) Solomon, S. *Rev. Geophys.* **1999**, *37*, 275−316.

(2) Solomon, S.; Garcia, R. R.; Rowland, F. S.; Wuebbles, D. J. *Nature* **1986**, *321*, 755.

(3) Tolbert, M. A.; Toon, O. B. *Science* **2001**, *292*, 61−63.

(4) Ravishankara, A. R. *Science* **1997**, *276*, 1058−1065.

(5) Luthy, R. G.; Aiken, G. R.; Brusseau, M. L.; Cunningham, S. D.; Gschwend, P. M.; Pignatello, J. J.; Reinhard, M.; Traina, S. J.; Weber, W. J., Jr.; Westall, J. C. *Environ. Sci. Technol.* **1997**, *31*, 3341−3347.

(6) Li, Y. Q.; Zhang, H. Z.; Davidovits, P.; Jayne, J. T.; Kolb, C. E.; Worsnop, D. R. *J. Phys. Chem. A* **2002**, *106*, 1220−1227.

(7) Corsi, S. R.; Hall, D. W.; Geis, S. W. *Environ. Toxicol. Chem.* **2001**, *20*, 1483−1490.

(8) Fisher, D. J.; Knott, M. H.; Turley, S. D.; Turley, B. S.; Yonkos, L. T.; Ziegler, G. P. *Environ. Toxicol. Chem.* **1995**, *14*, 1103−1111.

(9) Kent, R. A.; Andersen, D.; Caux, P.-Y.; Teed, S. *Environ. Toxicol.* **1999**, *14*, 481−522.

(10) Cramer, C. J.; Truhlar, D. G. *J. Am. Chem. Soc.* **1994**, *116*, 3892.

(11) Huneycutt, A. J.; Saykally, R. J. *Science* **2003**, *299*, 1329−1330.

(12) Liu, D.; Ma, G.; Levering, L. M.; Allen, H. C. *J. Phys. Chem. B* **2004**, *108*, 2252−2260.

(13) Ma, G.; Allen, H. *J. Phys. Chem. B* **2003**, *107*, 6343.

(14) Moad, A. J.; Simpson, G. J. *J. Phy. Chem. B* **2004**, *108*, 3548−3562 and references therein.

(15) Shen, Y. R. *Appl. Phys. B* **1999**, *68*, 295−300.

(16) Shultz, M. J.; Baldelli, S.; Schnitzer, C.; Simonelli, D. *J. Phys. Chem. B* **2002**, *106*, 5313−5324.

(17) Richmond, G. L. *Chem. Rev.* **2002**, *102*, 2693−2724.

(18) Hommel, E. L.; Allen, H. C. *J. Phys. Chem. B* **2003**, *107*, 10823−10828.

(19) Hommel, E. L.; Allen, H. C. *Analyst* **2003**, *128*, 750−755.

(20) Ma, G.; Allen, H. C. *J. Am. Chem. Soc.* **2002**, *124*, 9374−9375.

(21) Hirose, C.; Yamamoto, H.; Akamatsu, N.; Domen, K. *J. Phys. Chem.* **1993**, *97*, 10064−10069.

(22) Hirose, C.; Akamatsu, N.; Domen, K. *J. Chem. Phys.* **1992**, *96*, 997−1004.

(23) Hirose, C.; Akamatsu, N.; Domen, K. *Appl. Spectrosc.* **1992**, *46*, 1051−1072.

(24) Frisch, M. J.; Trucks, G. W.; Schlegel, H. B.; Scuseria, G. E.; Robb, M. A.; Cheeseman, J. R.; Zakrzewski, V. G.; Montgomery, J. A., Jr.; Stratmann, R. E.; Burant, J. C.; Dapprich, S.; Millam, J. M.; Kudin, K. N.; Strain, M. C.; Farkas, O.; Tomasi, J.; Barone, V.; Cossi, M.; Cammi, R.; Mennucci, B.; Pomelli, C.; Adamo, C.; Clifford, S.; Ochterski, J.; Petersson, G. A.; Ayala, P. Y.; Cui, Q.; Morokuma, K.; Malick, D. K.; Rabuck, A. D.; Raghavachari, K.; Foresman, J. B.; Cioslowski, J.; Ortiz, J. V.; Stefanov, B. B.; Liu, G.; Liashenko, A.; Piskorz, P.; Komaromi, I.; Gomperts, R.; Martin, R. L.; Fox, D. J.; Keith, T.; Al-Laham, M. A.; Peng, C. Y.; Nanayakkara, A.; Gonzalez, C.; Challacombe, M.; Gill, P. M. W.; Johnson, B.; Chen, W.; Wong, M. W.; Andres, J. L.; Gonzalez, C.; Head-Gordon, M.; Replogle, E. S.; Pople, J. A. *Gaussian 98*, revision A.11; Gaussian Inc.: Pittsburgh, PA, 2001.

(25) Mohamadi, F.; Richards, N. G. J.; Guida, W. C.; Liskamp, R.; Lipton, M.; Caufield, C.; Chang, G.; Hendrickson, T.; Still, W. C. *J. Comput. Chem.* **1990**, *11*, 440.

(26) McCarren, P. R. *Conformole*; The Ohio State University: Columbus, OH.

(27) Becke, A. D. *Phys. Rev. A* **1988**, *38*, 3098.

(28) Becke, A. D. *J. Chem. Phys.* **1993**, *98*, 5648.

(29) Lee, C.; Yang, W.; Parr, R. G. *Phys. Rev. B* **1988**, *37*, 785.

(30) Callam, C. S.; Singer, S. J.; Lowary, T. L.; Hadad, C. M. *J. Am. Chem. Soc.* **2001**, *123*, 11743.

(31) Scott, A. P.; Radom, L. *J. Phys. Chem.* **1996**, *100*, 16502−16513.

(32) Lu, R.; Gan, W.; Wu, B.-h.; Chen, H.; Wang, H.-f. *J. Phy. Chem. B* **2004**, *108*, 7297−7306.

(33) Hommel, E. L.; Ma, G.; Allen, H. C. *Anal. Sci.* **2001**, *17*, 1325−1329.

(34) Surface mole fraction of 0.50 and 0.33 EG corresponds to 0.40 and 0.29 EG mole fractions, respectively, and were calculated from the surface tension measurements using Gibbs equations as they relate to surface excess (also see ref 43).

(35) Buckley, P.; Giguere, P. A. *Can. J. Chem.* **1967**, *45*, 397−407.

(36) Sawodny, W.; Niedenzu, K.; Dawson, D. W. *Spectrochim. Acta A* **1967**, *23A*, 799−806.

(37) Bultinck, P.; Goeminne, I. G.; Van De Vondel, D. *J. Mol. Struct. (THEOCHEM)* **1995**, *357*, 19.

(38) Csonka, G. I.; Csizmadia, I. G. *Chem. Phys. Lett.* **1995**, *243*, 419.

(39) Radom, L.; Lathan, W. A.; Hehre, W. J.; Pople, J. A. *J. Am. Chem. Soc.* **1973**, *95*, 693.

(40) Oie, T.; Topol, I. A.; Burt, S. K. *J. Phys. Chem.* **1994**, *98*, 1121.

(41) Teppen, B. J.; Cao, M.; Frey, R. F.; van Alsenoy, C.; Miller, D. M.; Schafer, L. *J. Mol. Struct. (THEOCHEM)* **1994**, *120*, 169.

(42) Chaudhari, A.; Lee, S. *J. Chem. Phys.* **2004**, *120*, 7464−7469.

(43) Guggenheim, E. A.; Adam, N. K. *Proc. R. Soc.* **1933**, *A139*, 218.